PERGAMON

International Journal of Solids and Structures 40 (2003) 3229–3251

INTERNATIONAL JOURNAL OF SOLIDS and STRUCTURES

www.elsevier.com/locate/ijsolstr

Stability and vibration of empty and fluid-filled circular cylindrical shells under static and periodic axial loads

F. Pellicano [a,*], M. Amabili [b]

[a] Dip. di Ingegneria Meccanica e Civile, Università di Modena e Reggio Emilia, V. Vignolese, 905, Modena I-41100, Italy
[b] Dip. di Ingegneria Industriale, Università di Parma, Area delle Scienze, 181/A, Parma 43100, Italy

Received 28 September 2002; received in revised form 20 January 2003

Abstract

In the present study, the dynamic stability of simply supported, circular cylindrical shells subjected to dynamic axial loads is analysed. Geometric nonlinearities due to finite-amplitude shell motion are considered by using the Donnell's nonlinear shallow-shell theory. The effect of structural damping is taken into account. A discretization method based on a series expansion involving a relatively large number of linear modes, including axisymmetric and asymmetric modes, and on the Galerkin procedure is developed. Axisymmetric modes are included; indeed, they are essential in simulating the inward deflection of the mean oscillation with respect to the equilibrium position and in describing the axisymmetric deflection due to axial loads. A finite length, simply supported shell is considered; the boundary conditions are satisfied, including the contribution of external axial loads acting at the shell edges. The effect of a contained liquid is investigated. The linear dynamic stability and nonlinear response are analysed by using continuation techniques and direct simulations.

Keywords: Stability; Vibration; Axial loads

1. Introduction

The fundamental investigation on the stability of circular cylindrical shells is due to Von Kármán and Tsien (1941), who analysed the static stability (buckling) and the postcritical behaviour of axially loaded shells. In this study, the role of the sub-critical bifurcation of the equilibrium in the inaccuracy of the linear theories was explained. It was explained that linear analyses are not able to predict the actual buckling phenomenon observed in experiments; in particular, nonlinear analyses show that the bifurcation path is strongly sub-critical, therefore, safe design information can be obtained with a nonlinear analysis only. After this important contribution, many other studies have been published on static and dynamic stability of shells. A short literature overview is provided in the following.

* Corresponding author. Tel.: +39-059-2056154; fax: +39-059-2056129.
E-mail addresses: frank@unimo.it (F. Pellicano), marco@me.unipr.it (M. Amabili).

0020-7683/03/$ - see front matter © 2003 Elsevier Science Ltd. All rights reserved.
doi:10.1016/S0020-7683(03)00120-3

Roth and Klosner (1964) analysed the buckling of circular shells subjected to a suddenly applied load, using the Donnell's nonlinear shallow-shell theory. They noted that the presence of initial geometric imperfections largely reduce the critical load. A similar problem was analysed by Tamura and Babcok (1975) using the same theory; in this work it is shown that, in the case of step loading, the effect of in-plane inertia can reduce the critical load.

Vijayaraghavan and Evan-Iwanowski (1967) analysed both analytically and experimentally the parametrical instabilities of a circular shell under seismic excitation. The cylinder position was vertical and the base was axially excited by using a shaker. In this problem, the in-plane inertia is variable along the shell axis and, when the base is harmonically excited, gives rise to a parametric excitation. Instability regions are found analytically and compared to experimental results.

Koval (1974) used the Donnell's nonlinear shallow-shell theory to study the effect of a longitudinal resonance in the parametric transversal instability of a circular shell. He found that, combined parametric resonances give rise to complex regions of parametric instability. However, this kind of phenomenon was found at very high frequency and no damping was included in the analysis. Hsu (1974) used the Donnell's linear shallow-shell theory to analyse the parametric instability of a circular cylindrical shell: a uniform pressure load and an axial dynamic load were considered, the former was added in order to eliminate the Poisson's effect in the in-plane stresses. The same problem was studied by Nagai and Yamaki (1978) using the Donnell's linear shallow-shell theory, considering different boundary conditions. In this work, the effect of axisymmetric bending vibrations induced by the axial load and essentially due to the Poisson's effect was considered. The classical membrane approach for the in-plane stresses was found inaccurate when the vibration amplitude of axisymmetric modes is not negligible.

Greenberg and Stavsky (1980) analysed the natural frequencies of orthotropic composite, axially compressed, cylindrical shells using the Love's shell theory.

Koval'chuk and Krasnopol'skaya (1980) considered the effect of geometric imperfection, using the Donnell's nonlinear shallow-shell theory and a simple three-mode expansion, which included driven and companion mode, also referred as "conjugate form" (the symmetry of the shell gives rise to two asymmetric modes having the same frequency and the same waveform, but shifted circumferentially of 1/4 wave length; these two modes are named driven and companion modes or conjugated forms). Viscous material dissipation was considered. In this work the fundamental role of initial geometric imperfections is analysed.

Croll and Batista (1981) established lower bounds for static buckling of very long and thin-walled, axially loaded cylindrical shells, using the Donnell's theory.

Bert and Birman (1988) studied the parametric instability of thick circular shells, developing a special version of the Sanders–Koiter thin-shell theory for thick shells. A single mode analysis, giving rise to a Mathieu type equation of motion, allowed to determine the instability regions.

Argento (1993) used the Donnell's linear theory and the classical lamination theory to study the dynamic stability of composite circular clamped–clamped shells under axial and torsional loading. The linear equations of motion, obtained from discretization, are analysed by means of the harmonic balance method and the linear instability regions were found. Argento and Scott (1993a,b) studied the dynamic stability of layered anisotropic circular cylindrical shells.

Popov et al. (1998) analysed the parametric stability and the postcritical behaviour of an infinitely long circular cylindrical shell, dropping the boundary conditions. A three-mode expansion was used, without the inclusion of the companion mode. Membrane theory was used to evaluate the in-plane stresses due to the axial load. The effect of internal resonances between asymmetric modes was analysed in detail.

Gonçalves and Del Prado (2000, 2002) analysed the dynamic buckling of a perfect circular cylindrical shell under axial static and dynamic loads. Donnell's nonlinear shallow-shell theory was used and the membrane theory was considered to evaluate the in-plane stresses. The partial differential operator was discretized through the Galerkin technique, using a relatively large modal expansion. However, no companion mode participation was considered and the boundary conditions were dropped by assuming an

infinitely long shell. Escape from potential well was analysed in detail, and a correlation of this phenomenon with the parametric resonance was given.

Apart from the previously mentioned papers, which are strictly related to the object of the present paper, other interesting studies on nonlinear vibrations of shells deserve to be commented. The inclusion of the companion mode in the flexural displacement can be attributed to Evensen (1967) and Dowell and Ventres (1968); the importance of these studies is also due to the inclusion of axisymmetric terms.

The literature regarding large-amplitude nonlinear vibrations of shells with fluid–structure interactions is not wide; see e.g. the literature review on the nonlinear dynamics of shells in vacuo, filled with or surrounded by quiescent and flowing fluids by Amabili and Païdoussis (2003). The effect of a contained still heavy fluid is considered by Gonçalves and Batista (1988) and by Amabili et al. (1998). The nonlinear dynamics and stability of shells containing flowing fluid is analysed in Amabili et al. (1999a,b, 2000a,b). An accurate convergence test can be found in Pellicano et al. (2002) where the dependence of the type of nonlinearity on the shell geometry is analysed in detail. In Kubenko et al. (1982) an interesting review on the subject can be found.

In the present paper, the dynamic stability and postcritical dynamics of a circular cylindrical shell subjected to periodic and static axial loads is analysed. The Donnell's nonlinear shallow-shell theory is used; the effect of a contained fluid is considered and simply supported boundary conditions are satisfied. The transversal flexural displacement is expanded using linear vibration modes. The expansion is suitably truncated in order to ensure the convergence; asymmetric companion modes and axisymmetric modes are included. The dynamics of axisymmetric modes is considered, avoiding the approximation of the membrane theory for the in-plane stress evaluation. The dynamical system obtained through a Galerkin procedure is analysed with numerical techniques. In particular, a software for the continuation and bifurcation of solutions of ordinary differential equations is used (Doedel et al., 1998) for the analysis of static and periodic solutions; direct simulations are performed for nonstationary responses. Time histories, spectra, phase spaces and bifurcation diagrams of the Poincaré maps are shown for the most interesting cases.

2. Governing equations

In this study, a detailed analysis of the nonlinear dynamics of simply supported, complete circular cylindrical shells of finite length L is made. In order to describe the geometry of the shell, a cylindrical coordinate system $(O; x, r, \theta)$ is considered, where O is the origin placed at the centre of one end of the shell, x is the axial and r is the radial coordinate. The displacement field of the middle surface of the shell is given by the following components: u, v and w; in the axial, circumferential and radial directions, respectively. Initial imperfections are not considered here, but the structural model developed by the authors of the present paper has been successfully used in the case of imperfections. Therefore, the present analysis could be easily extended to this important case.

The Donnell's nonlinear shallow-shell theory is used. The equation of motion for finite-amplitude, flexural vibrations of a thin, circular cylindrical shell is given by (Evensen, 1967; Amabili et al., 1998, 1999a)

$$D\nabla^4 w + ch\dot{w} + \rho h\ddot{w} = f + p + \frac{1}{R}\frac{\partial^2 F}{\partial x^2} + \left(\frac{\partial^2 F}{R^2\partial\theta^2}\frac{\partial^2 w}{\partial x^2} - 2\frac{\partial^2 F}{R\partial x\partial\theta}\frac{\partial^2 w}{R\partial x\partial\theta} + \frac{\partial^2 F}{\partial x^2}\frac{\partial^2 w}{R^2\partial\theta^2}\right) \tag{1}$$

with the compatibility equation

$$\frac{1}{Eh}\nabla^4 F = -\frac{1}{R}\frac{\partial^2 w}{\partial x^2} + \left[\left(\frac{\partial^2 w}{R\partial x\partial\theta}\right)^2 - \frac{\partial^2 w}{\partial x^2}\frac{\partial^2 w}{R^2\partial\theta^2}\right], \tag{2}$$

where $D = Eh^3/[12(1-\nu^2)]$ is the flexural stiffness, E is Young's modulus, ν the Poisson ratio, h the shell thickness, R the mean shell radius, ρ the mass density of the shell, c the damping coefficient. The radial

deflection w is positive inward, $\dot{w} = (\partial w/\partial t)$ and $\ddot{w} = (\partial^2 w/\partial t^2)$; F is the in-plane stress function. In Eqs. (1) and (2) the biharmonic operator is defined as $\nabla^4 = [\partial^2/\partial x^2 + \partial^2/(R^2\partial\theta^2)]^2$, p is the pressure acting on the shell surface due to the fluid–structure interaction and f is a distributed external load that is not included in the following ($f = 0$). By using Donnell's nonlinear shallow-shell theory, the results are accurate only for modes of high circumferential wave number n (n is the number of nodal diameters); specifically, $1/n^2 \ll 1$ must be satisfied, which implies the condition $n \geqslant 5$, in order to have fairly good accuracy. The in-plane inertia is neglected. The forces per unit length in the axial and circumferential directions, as well as the shear force, are given by (Evensen, 1967; Amabili et al., 1998, 1999a)

$$N_x = \frac{1}{R^2}\frac{\partial^2 F}{\partial\theta^2}, \quad N_\theta = \frac{\partial^2 F}{\partial x^2}, \quad N_{x\theta} = -\frac{1}{R}\frac{\partial^2 F}{\partial x \partial\theta}. \tag{3}$$

The force–displacement relations are

$$(1-\nu^2)\frac{N_x}{Eh} = -\frac{\nu w}{R} + \frac{1}{2}\left(\frac{\partial w}{\partial x}\right)^2 + \frac{\nu}{2}\left(\frac{\partial w}{R\partial\theta}\right)^2 + \frac{\partial u}{\partial x} + \frac{\nu}{R}\frac{\partial v}{\partial\theta}, \tag{4}$$

$$(1-\nu^2)\frac{N_\theta}{Eh} = -\frac{w}{R} + \frac{\nu}{2}\left(\frac{\partial w}{\partial x}\right)^2 + \frac{1}{2}\left(\frac{\partial w}{R\partial\theta}\right)^2 + \nu\frac{\partial u}{\partial x} + \frac{1}{R}\frac{\partial v}{\partial\theta}, \tag{5}$$

$$(1-\nu^2)\frac{N_{x\theta}}{Eh} = 2(1-\nu)\left[\frac{1}{R}\frac{\partial w}{\partial x}\frac{\partial w}{\partial\theta} + \frac{1}{R}\frac{\partial u}{\partial\theta} + \frac{\partial v}{\partial x}\right]. \tag{6}$$

The following simply supported boundary conditions are considered:

$$\left.\begin{array}{l} w = 0 \\ M_x = -D\{(\partial^2 w/\partial x^2) + \nu[\partial^2 w/(R^2\partial\theta^2)]\} = 0 \end{array}\right\} \quad \text{at } x = 0, L, \tag{7a}$$

$$N_x = \widetilde{N}_x(t) \quad \text{at } x = 0, L \quad \text{and} \quad v = 0 \quad \text{at } x = 0, L. \tag{7b}$$

Moreover, the condition that u, v and w are continuous in θ is imposed.

The axial load is periodic and presents a mean negative value (compressive load): $\widetilde{N}_x(t) = -N + N_D\cos\omega t$. The radial displacement w is expanded by using the linear shell eigenmodes as basis; in particular, the flexural response may be written as follows:

$$\begin{aligned} w(x,\theta,t) = &\sum_{n_1=1}^{N_1}\sum_{m=1}^{N_1}[A_{m,(n_1 n)}(t)\cos(n_1 n\theta) + B_{m,(n_1 n)}(t)\sin(n n_1\theta)]\sin(\lambda_m x) \\ &+ \sum_{m=1}^{M} A_{2m-1,0}(t)\sin(\lambda_{2m-1}x), \end{aligned} \tag{8}$$

where $\lambda_m = m\pi/L$, t is the time; $A_{m,j}(t)$, $B_{m,j}(t)$ and $A_{m,0}(t)$ are unknown functions of t and $j = n_1 n$. In the numerical calculations, N_1 and M will be assigned equal to 3 and 5, respectively. Expansion (8) is suggested by the presence of quadratic and cubic nonlinearities. When a linear mode $(1, n)$ is excited, the quadratic nonlinearity gives coupling with modes having $2n$ circumferential waves, 2 longitudinal half-waves and with axisymmetric modes, while the cubic nonlinearity gives coupling with modes having $3n$ circumferential waves and 3 longitudinal half-waves. Further coupling with different asymmetric modes, which can arise when internal resonances are present, are not considered here. For simplicity modes associated to generalized coordinates $A_{m,j}(t)$ and $B_{m,j}(t)$ are referred as driven and companion modes, respectively, even if in this case the asymmetric modes are not directly driven by external excitation.

Some tests including axisymmetric modes with an even m in the expansion showed that they are never excited. Mode expansion (8) may be considered the most complete expansion in absence of modal interactions due to internal resonance and a nonsymmetric spatial excitation. Note that a particular care must be given to the axisymmetric modes in order to describe correctly the outward axial–symmetric deflection due to the compressive load before buckling. For the problem analysed in this paper, the series practically converges with the ninth axisymmetric mode.

2.1. Particular solution of the stress function

Let us consider the most general form of the displacement expansion:

$$w = \sum_{m=1}^{M} \sum_{n=0}^{\widehat{N}} (A_{mn} \cos n\theta + B_{mn} \sin n\theta) \sin m\eta, \tag{9}$$

where $\eta = \pi x/L$ and $\widehat{N} = nN_1$. Expansion (9) can be reduced to Eq. (8) by suitably eliminating extra terms.

Substituting the expansion of w, Eq. (9), into the right-hand side of Eq. (2), a partial differential equation for the stress function F is obtained, the solution of which may be written as

$$F = F_{\mathrm{h}} + F_{\mathrm{p}}, \tag{10}$$

where F_{h} is the homogeneous and F_{p} is the particular solution. The following general expression for the particular solution can be found:

$$F_{\mathrm{p}} = \sum_{m=0}^{2M} \sum_{n=0}^{\widehat{2N}} (F_{mn1} \sin m\eta \sin n\theta + F_{mn2} \sin m\eta \cos n\theta + F_{mn3} \cos m\eta \sin n\theta + F_{mn4} \cos m\eta \cos n\theta), \tag{11}$$

where the coefficients $F_{mn,i}$, $i = 1, \ldots, 4$, have long expressions not reported.

The homogeneous solution is obtained in the next section by imposing the boundary conditions.

2.2. Boundary conditions

The boundary conditions given by Eqs. (7a) are exactly respected by the expansion of the transversal displacement field w; such expansion satisfies the continuity of circumferential displacement (Amabili et al., 1998, 1999a). The homogeneous part of the stress function allows to satisfy on the average the in-plane boundary conditions (7b):

$$\int_0^{2\pi} N_x R \, \mathrm{d}\theta = 2\pi R \widetilde{N}_x(t), \tag{12a}$$

$$\int_0^{2\pi} \int_0^{L} N_{x\theta} \, \mathrm{d}x R \, \mathrm{d}\theta = 0. \tag{12b}$$

In particular, Eq. (12a) imposes that the external load $\widetilde{N}_x$ is equal to the in-plane axial stress N_x averaged circumferentially; Eq. (12b) can be satisfied when u and w are continuous in θ on the average, and $v = 0$ on the average at $x = 0, L$. The use of the averaged boundary conditions (12a, b) allows to evaluate an analytical approximation of the stress function. The use of this approximation is quite common in the literature regarding nonlinear vibrations of shells (Dowell and Ventres, 1968; Amabili et al., 1999a,b, 2000a,b; Kubenko et al., 1982).

It can be proven that, the displacement expansion of w and the solution of the stress function allows to satisfy exactly the circumferential continuity of the displacement field v:

$$\int_0^{2\pi} \frac{\partial v}{\partial \theta} \mathrm{d}\theta = \int_0^{2\pi} \left[\frac{1}{Eh} \left(\frac{\partial^2 F}{\partial x^2} - \nu \frac{\partial^2 F}{R^2 \partial \theta^2} \right) + \frac{w}{R} - \frac{1}{2} \left(\frac{\partial w}{R \partial \theta} \right)^2 \right] \mathrm{d}\theta = 0. \tag{13}$$

The homogeneous solution of Eq. (2) may be assumed to be of the form (Amabili et al., 1999a,b, 2000a,b,c; Pellicano et al., 2000; Amabili and Pellicano, 2002)

$$F_{\mathrm{h}} = \frac{1}{2} \overline{N}_x R^2 \theta^2 + \frac{1}{2} x^2 \left\{ \overline{N}_\theta - \frac{1}{2\pi RL} \int_0^L \int_0^{2\pi} \left[\frac{\partial^2 F_{\mathrm{p}}}{\partial x^2} \right] R \, \mathrm{d}\theta \, \mathrm{d}x \right\} - \overline{N}_{x\theta} x R \theta, \tag{14}$$

where $\overline{N}_x$, $\overline{N}_\theta$ and $\overline{N}_{x\theta}$ are the average in-plane restraint stresses generated at the ends of the shell, as a consequence of the in-plane constraints on the average and the external axial load. Eq. (14) is chosen in order to satisfy the boundary conditions on the average. Boundary conditions (12) allow to express the in-plane restraint stresses $\overline{N}_x$, $\overline{N}_\theta$ and $\overline{N}_{x\theta}$ in terms of w and its derivatives, see Eqs. (4)–(6)

$$\overline{N}_x = \widetilde{N}_x, \tag{15}$$

$$\overline{N}_\theta = \nu \widetilde{N}_x + \frac{Eh}{2\pi L} \int_0^{2\pi} \int_0^L \left[-\frac{w}{R} + \frac{1}{2} \left(\frac{\partial w}{R \partial \theta} \right)^2 \right] \mathrm{d}x \, \mathrm{d}\theta, \tag{16}$$

$$\overline{N}_{x\theta} = 0. \tag{17}$$

In particular, N_θ is given by

$$N_\theta = \nu \widetilde{N}_x + \frac{Eh}{2\pi^2 R} \left\{ 2\pi \sum_{m=1}^{M} \frac{A_{m0}}{m} [(-1)^m - 1] + \frac{\pi^2}{4R} \sum_{m=1}^{M} \sum_{n=0}^{N} n^2 (A_{mn}^2 + B_{mn}^2) \right\}. \tag{18}$$

3. Fluid–structure interaction

The shell is assumed to be empty or completely fluid-filled. An incompressible inviscid fluid is considered and the effect of the dynamic pressure acting on the shell surface is linearized (Gonçalves and Batista, 1988; Lakis and Laveau, 1991); the gravity effect is neglected. The fluid velocity field can be described in terms of the velocity potential Φ, by means of the Laplace equation:

$$\nabla^2 \Phi = \frac{\partial^2 \Phi}{\partial x^2} + \frac{\partial^2 \Phi}{\partial r^2} + \frac{1}{r} \frac{\partial \Phi}{\partial r} + \frac{1}{r^2} \frac{\partial^2 \Phi}{\partial \theta^2} = 0. \tag{19}$$

The fluid velocity field is given by $\mathbf{v} = -\nabla \Phi$. If no cavitation is present, one can write:

$$\left(\frac{\partial \Phi}{\partial r} \right)_{r=R} = \dot{w}. \tag{20}$$

Open ends are considered at the shell edges, i.e., zero pressure at both ends:

$$(\Phi)_{x=0} = (\Phi)_{x=L} = 0 \tag{21}$$

and the linearized Bernoulli equation give the fluid pressure:

$$p = \rho_{\mathrm{F}} \frac{\partial \Phi}{\partial t}. \tag{22}$$

The solution of Eq. (19) and therefore the fluid pressure p can be easily obtained in terms of Bessel functions and is not reported here for the sake of brevity (see Amabili et al., 1998, 1999a for details).

4. Discretized equations

When the stress function and the fluid effect are evaluated, the classical Galerkin approach can be applied. The expansion of w given by Eq. (8), the stress function given by Eq. (10) and the fluid pressure p are substituted into Eq. (1) and the result is projected on the basis (8).

The resulting discrete equations of motion are a set of 2nd order, nonlinear ordinary differential equations linearly uncoupled:

$$\ddot{A}_{m,n}(t) + 2\zeta_{mn}\omega_{mn}\dot{A}_{m,n}(t) + \omega_{mn}^2 A_{m,n}(t) + \gamma_{mn}(t)A_{m,n}(t) + g_{2,1}^{(A,m,n)} + g_{2,2}^{(A,m,n)} + g_{3,1}^{(A,m,n)} + g_{3,2}^{(A,m,n)} = 0, \tag{23}$$

$$\ddot{B}_{m,n}(t) + 2\zeta_{mn}\omega_{mn}\dot{B}_{m,n}(t) + \omega_{mn}^2 A_{m,n}(t) + \gamma_{mn}(t)B_{m,n}(t) + g_{2,1}^{(B,m,n)} + g_{2,2}^{(B,m,n)} + g_{3,1}^{(B,m,n)} + g_{3,2}^{(B,m,n)} = 0, \tag{24}$$

$$\ddot{A}_{m,0}(t) + 2\zeta_{m0}\omega_{m0}\dot{A}_{m,0}(t) + \omega_{m0}^2 A_{m,0}(t) + \gamma_{m0}(t)A_{m,0}(t) + g_{2,1}^{(m,0)} + g_{2,2}^{(m,0)} + g_{3,1}^{(m,0)} + g_{3,2}^{(m,0)} + r_{m,0}(t) = 0, \tag{25}$$

where $g_{2,1}^{(A,m,n)}$, $g_{2,1}^{(B,m,n)}$ and $g_{2,1}^{(A,m,0)}$ are quadratic functions of the asymmetric modal coordinates $A_{1,n}, \ldots, B_{1,n}, \ldots$; $g_{2,2}^{(A,m,n)}$, $g_{2,2}^{(B,m,n)}$ and $g_{2,2}^{(A,m,0)}$ are quadratic functions of all modal coordinates $A_{1,n}, \ldots, B_{1,n}, \ldots$ and $A_{1,0}, \ldots$; $g_{3,1}^{(A,m,n)}$, $g_{3,1}^{(B,m,n)}$ and $g_{3,1}^{(A,m,0)}$ are cubic functions of the asymmetric modal coordinates $A_{1,n}, \ldots, B_{1,n}, \ldots$; $g_{3,2}^{(A,m,n)}$, $g_{3,2}^{(B,m,n)}$ and $g_{3,2}^{(A,m,0)}$ are cubic functions of all modal coordinates $A_{1,n}, \ldots, B_{1,n}, \ldots$ and $A_{1,0}, \ldots$

Eqs. (23)–(25) are referred to asymmetric modes (conjugate modes $A_{m,n}$ and $B_{m,n}$) and axisymmetric modes. The parametric excitation is given by the parameters $\gamma_{m,n}$ and $\gamma_{m,0}$. In Eq. (24), the term $r_{m,0}(t)$ is a direct excitation due to the axial load through the Poisson's effect. Note that the direct excitation is present only in the axisymmetric modal equations. When the system is excited, Eqs. (22) and (23) can have trivial solution; conversely, Eq. (24), which is directly forced, presents a nontrivial solution. Therefore, the following solution are admissible: $A_{m,n} = 0$, $B_{m,n} = 0$, $A_{m,0} \neq 0$. The excitation of axisymmetric modal coordinates furnishes a further parametric excitation on the asymmetric modal equations through the nonlinear coupling.

5. Numerical results

A numerical analysis is performed on a test shell, studied in Popov et al. (1998) and Gonçalves and Del Prado (2000), having the following characteristics: $h = 2 \times 10^{-3}$ m, $R = 0.2$ m, $L = 0.4$ m, $E = 2.1 \times 10^{11}$ N/m^2, $v = 0.3$, $\rho = 7850$ kg/m^3; in the case of fluid-filled shell, $\rho_F = 1000$ kg/m^3. In order to compare the model developed in the present study with results present in literature, some tests are performed adopting both the simple modal viscous damping and the Kelvin–Voight damping model used in Popov et al. (1998) and Gonçalves and Del Prado (2000), which gives, for example, $\zeta = 0.089$ on mode ($m = 1$, $n = 5$); such value of damping is quite high, however, it could be due, for example, to support dissipation. Experiments available in literature indicate lower damping ratio for steel shells (see e.g. Amabili et al., 2002). Therefore, the following damping ratios are also considered: $\zeta = 0.0008$ for empty shell and $\zeta = 0.003$ for fluid-filled shell.

The fundamental frequency of the empty shell is equal to $2\pi \times 503.7$ rad/s and is obtained for $m = 1$ and $n = 5$. The most interesting modes, for the present study, are listed in Table 1 (empty shell) and Table 2 (water-filled shell).

Table 1
Linear natural frequencies for the empty shell (rad/s)

$\omega_{1,5} = 3165.03$	$\omega_{3,5} = 12713.9$	$\omega_{1,10} = 8043.12$	$\omega_{3,10} = 10655.9$
$\omega_{1,15} = 17803.5$	$\omega_{3,15} = 19485.1$	$\omega_{1,0} = 25861.7$	$\omega_{3,0} = 25919.3$
$\omega_{5,0} = 26307.7$	$\omega_{7,0} = 27537.5$	$\omega_{9,0} = 30222.9$	

Table 2
Linear natural frequencies for the water-filled shell (rad/s)

$\omega_{1,5} = 1704.36$	$\omega_{3,5} = 7446.14$	$\omega_{1,10} = 5350.42$	$\omega_{3,10} = 7248.34$
$\omega_{1,15} = 13107.4$	$\omega_{3,15} = 14473.5$	$\omega_{1,0} = 6856.61$	$\omega_{3,0} = 12879.1$
$\omega_{5,0} = 15902.9$	$\omega_{7,0} = 18502$	$\omega_{9,0} = 21728$	

5.1. Static bifurcation analysis

A static compressive axial load is considered. It is well known that, when a circular cylindrical shell is axially compressed, a catastrophic sub-critical bifurcation can occur (Von Kármán and Tsien, 1941).

The classical critical load per unit length in the circumferential direction is given by (Yamaki, 1984) $N_{cr} = Eh^2/(R\sqrt{3(1-\nu^2)})$, for the present case N_{cr} is obtained for $m = 1$, $n = 5$ and assumes the value $N_{cr} = 2.54 \times 10^6$ N/m.

When the axial load reaches the critical load, the trivial equilibrium position loses stability, branch 1 of Fig. 1, and the shell suddenly collapses into a deformed configuration. Indeed, the bifurcation branch, which starts from the bifurcation point, is strongly sub-critical (branch 2 in Fig. 1), i.e., stable bifurcated configurations exist before the critical load. In particular, four bifurcated configurations exist for each value of the axial load when $N/N_{cr} \in [0.2, 1]$; two branches are stable (thick lines) and the others are unstable (thin lines). A folding is present at $N/N_{cr} \cong 0.2$, this is extremely important in practical applications; indeed, the structure can collapse below the critical load, as underlined in Von Kármán and Tsien (1941), when perturbations are present. It is useful to clarify that the word "perturbations" indicates all kind of perturbing factors: energy furnished through impacts, transversal or axial periodic excitations, geometric imperfections. The present results have been obtained with the continuation software AUTO by means of a

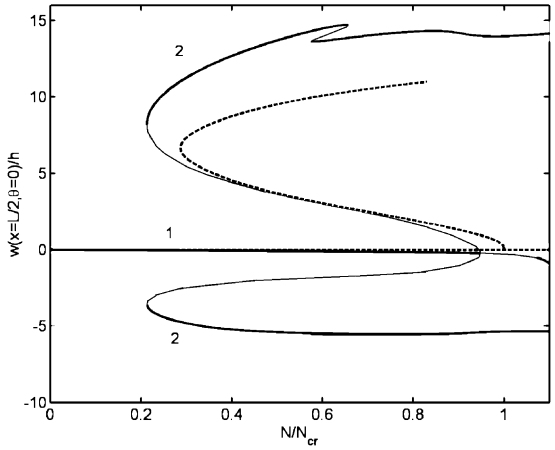

Fig. 1. Static bifurcation (empty shell): (━) stable solution, (—) unstable solution, (- - -) Gonçalves and Del Prado (2000). Prebuckling, 1st branch; postbuckling, 2nd branch.

17 dof model including 5 axisymmetric modes. The present solution is compared with that obtained in Gonçalves and Del Prado (2000) (dotted line), showing a good agreement in the bifurcation path. Note that the present model predicts bifurcation when the axial load is 95% of the classical load N_{cr}; it is well known that the classical critical load overestimates the actual critical load, because it refers to infinitely long shells. In the case of finite long shells the well known "prebuckling effect" (Yamaki, 1984) reduces the critical load.

It is worthwhile to stress that the present results have been obtained by respecting the simply supported boundary conditions for a finite length shell; conversely, in Gonçalves and Del Prado (2000) an infinitely long shell is considered; this can explain the differences in the results.

Moreover, it is interesting to note that, when the shell is compressed, the Poisson's effect induces an expansion of the surface, see the first branch of the unbuckled structure (w is positive inward); this effect is due to the axisymmetric modes, which are directly forced by the static axial load through the Poisson's effect. The axisymmetric contribution causes also the asymmetry of inward and outward branches; Fig. 1 shows that the shell is weaker inward (larger deformation of the positive part of branch 2).

5.2. Dynamic bifurcation analysis

When the shell is excited by an axial periodic load, two kind of excitations are present on the modal equations: (i) a direct excitation of the axisymmetric modes due to the Poisson's effect; (ii) a parametric excitation of all modes. However, the direct excitation of axisymmetric modes induces a further parametric excitation on the asymmetric modes due to the nonlinear coupling with axisymmetric modes.

In many studies the in-plane stresses are evaluated by means of the membrane theory, i.e., the axisymmetric response is evaluated from a static analysis. This approach can give inaccurate results when the axisymmetric modes undergoes to a resonance and both the amplitude and the phase of oscillation change (Nagai and Yamaki, 1978).

In order to compare the present model to Popov et al. (1998), the following conditions are considered: static load $N = 0$, Kelvin–Voight damping (damping ratio equal to 0.089 on the fundamental mode) and excitation frequency $\omega/\omega_{1,5} = 1.9$.

The numerical analysis is performed by means of continuation techniques (Doedel et al., 1998); such methods are not able to follow bifurcation surfaces, which arise in the presence of symmetric problems. Circular cylindrical shells under axial loads represent the typical problem where the geometric symmetry causes bifurcation surfaces; indeed, when the dynamic load reaches the critical amplitude, both modes having the "same shape" (represented circumferentially by sine and cosine functions) and frequency can bifurcate, giving rise to a bifurcation surface in the amplitudes-parameter space. Geometric imperfections are always present in actual shells; in particular, asymmetric imperfections split the natural frequencies of the two modes with the same number of circumferential waves. In the present model, geometric imperfections are not directly introduced, they are taken into account in a simplified way by introducing a 1% of difference in the natural frequencies of driven and companion modes. This frequency splitting allows to consider small geometric imperfections and to use continuation techniques.

When $\omega/\omega_{1,5} = 1.9$, the frequency of excitation is close to the principal parametric resonance of the fundamental mode. In Fig. 2(a)–(c) the maximum amplitudes of periodic oscillation are represented for modes $A_{1,5}$, $B_{1,5}$ and $A_{1,0}$ versus N_D/N_{cr}; even if in the calculation a larger set of modes is used, just few modes are shown, for the sake of brevity. Increasing the dynamic excitation level N_D, a period doubling bifurcation, due to a parametric instability, is found for $N_D/N_{cr} = 0.46$, see Fig. 2. Before the bifurcation the shell vibrates with the same frequency of excitation ($1T$ oscillation), and the dynamics is due to the axisymmetric modes only, see the figure included in Fig. 2(c) showing the shell deformation. After the period doubling bifurcation a sub-critical branch 2 can be observed. Branch 2 is initially unstable up to the folding, $N_D/N_{cr} = 0.409$; this branch loses stability and bifurcates at $N_D/N_{cr} = 0.49$, where the conjugate mode $B_{1,5}$ is excited and a travelling-wave response can appear. In Fig. 2(a) the asymmetric deformation of

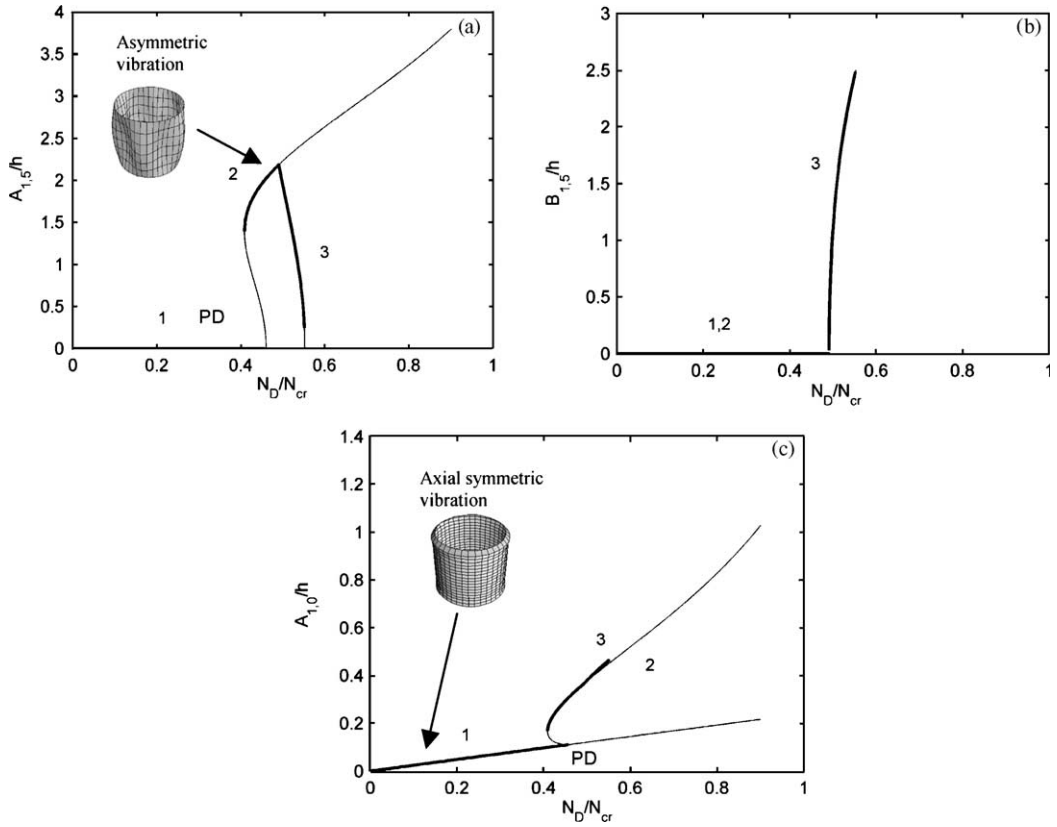

Fig. 2. Dynamic instability (empty shell): static load $N/N_{cr} = 0$, $\zeta = 0.089$. $\omega/\omega_{1,5} = 1.9$. (▬) stable solution, (—) unstable solution; 'PD' period doubling.

the shell is shown. When $N_D > 0.49$ no periodic solutions are found; this region must be investigated through a direct numerical integration, which allows to investigate nonstationary dynamics. For the same problem, in Popov et al. (1998) the parametric instability has been found at $N_D/N_{cr} = 0.39$. In order to explain this discrepancy the present model has been modified. The membrane theory has been used to evaluate the in-plane stresses. The analytical details are not reported here for the sake of brevity. However, an explanation of the effects could be useful. Using the membrane theory, the axisymmetric contribution is not included directly in the dynamics of the axisymmetric modes, i.e. these modes are not directly excited. The dynamic critical load, with this simplified approach, is $N_D/N_{cr} = 0.398$; the small difference with Popov et al. (1998) can be easily explained: even if the same simplification is followed for the evaluation of the in-plane stresses, here simply supported boundary conditions are respected; conversely, in Popov et al. (1998) infinitely long shells are considered; moreover, a larger set of modes is used in the present study.

In order to quantify the effect of a contained fluid and the damping, the dynamic critical loads are computed for different excitation frequencies, damping ratios and considering empty and water-filled shells; the results are reported in Table 3. It is of interest that the presence of a contained fluid enlarges the critical load; this safety effect is due only to the inertial effect of fluid. Indeed, in these simulations the damping ratio has been considered equal to 0.089 for all modes, except for the following cases: $\zeta = 0.016$ and the Kelvin–Voight model with $\zeta_{1,5} = 0.089$. The inertial fluid effect reduces the natural frequencies: in some conditions axisymmetric modes vibrate with larger amplitude and change the critical dynamic load. It must

Table 3
Critical dynamic load: the damping ratio is constant on all modes if not specified

N_D/N_{cr}	$\omega/\omega_{1,5}$	ζ	Presence of fluid
0.448	1.9	0.089	No
0.86	1.9	0.089	Yes
0.416	2	0.089	No
0.722	2	0.089	Yes
0.492	2.1	0.089	No
0.724	2.1	0.089	Yes
0.24	1.9	0.016	No
0.46	1.9	$\zeta_{1,5} = 0.089$[a]	No

[a] Kelvin–Voight damping model, Popov et al. (1998), Gonçalves and Del Prado (2000).

be pointed out that, using the membrane theory, the inertial effect cannot be included in the axisymmetric vibration. Therefore, in presence of fluid the membrane theory can give highly inaccurate results. From Table 3 one can observe that using a simple constant modal damping, the result do not change greatly with respect the Kelvin–Voight damping model. Moreover, it must be noted the strong influence of the damping ratio on the dynamic critical load: for $\zeta = 0.016$ the dynamic critical load is almost 50% smaller than the case $\zeta = 0.089$; this is a well known feature of the parametric resonance (Nayfeh and Mook, 1979), and can explain the importance of a correct estimate of the damping ratio in analysing parametric resonances.

The contribution of the axisymmetric modes, for the water-filled shell, in the present case is magnified by the vicinity of the resonance of the first axisymmetric mode. Indeed, in presence of water $\omega_{1,0}/\omega_{1,5} \cong 4$, see Table 2; therefore, when $\omega/\omega_{1,5} = 1.9$, case of Fig. 2, the resonance of the first axisymmetric mode is not far. In order to quantify this contribution, a simulation is performed by varying the excitation frequency. In Fig. 3 the maximum amplitude of the first axisymmetric mode is plotted versus the excitation frequency. For $\omega/\omega_{1,5} \cong 1.96$ an instability takes place, due to the parametric resonance of the fundamental mode; the response regains stability at $\omega/\omega_{1,5} \cong 2.14$; then the solution loses stability definitively at $\omega/\omega_{1,5} \cong 2.62$. When $\omega/\omega_{1,5} \in (1.96, 2.14)$, i.e. in the principal instability region, the axisymmetric mode amplitude is 30% higher then the static response at $\omega/\omega_{1,5} = 0$. Therefore, if the axisymmetric dynamics are neglected, in this case, an important part of the shell vibration is lost. It must be stressed that, the axisymmetric vibration causes a parametric excitation of asymmetric modes, because of the nonlinear coupling. Therefore, an

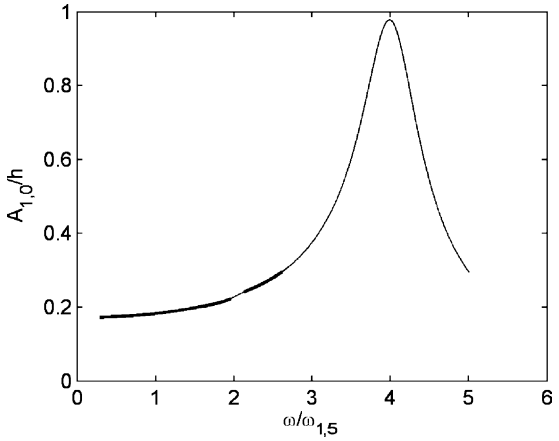

Fig. 3. Axisymmetric amplitude of oscillation (water-filled shell): $N/N_{cr} = 0$, $N_D/N_{cr} = 0.75$, $\zeta = 0.089$. (━) stable solution, (—) unstable solution.

inaccurate evaluation of this contribution leads to inaccurate findings on the parametric resonance detection.

In order to analyse the dynamic behaviour of the structure, without fluid, but in presence of a static component of the axial load, the following case is analysed: $N/N_{cr} = 0.8$, $\zeta = 0.089$ and $\omega/\omega_{1,5(0)} = 0.7$; where $\omega_{1,5(0)}$ is the frequency of the fundamental mode in the case of $N = 0$. Indeed, the linear natural frequencies decreases as the static compressive load N increases. In this case, the actual free oscillation frequency is one half the excitation frequency and a parametric resonance can be met. In Fig. 4(a) and (b) the maximum amplitude of modes $A_{1,5}$ and $A_{1,0}$ are represented. Large instability regions are found for $N_D/N_{cr} \in (0.142, 0.355)$ and $N_D/N_{cr} > 0.392$; after $N_D/N_{cr} = 0.392$ no periodic or trivial solutions are generally stable, except for extremely small regions. Furthermore, period doublings are observed for $N_D/N_{cr} \in (0.47, 0.4703)$. Note that in Gonçalves and Del Prado (2000) the first instability is found at $N_D/N_{cr} \approx 0.15$, i.e. very close to the present results; but the postcritical scenario was completely different.

It is now interesting to investigate the results obtained with the membrane theory. The first main difference with the previous results is that axisymmetric modes are not directly excited, before the bifurcation all modes have trivial amplitude, Fig. 5(a) and (b). The critical load is found at $N_D/N_{cr} = 0.2235$, where a $2T$ sub-harmonic bifurcation (branch 2) appears. A folding is present in branch 2 at $N_D/N_{cr} = 0.1355$; the 1/2 sub-harmonic solution loses stability at $N_D/N_{cr} = 0.156$, where a bifurcation branch 3, including the

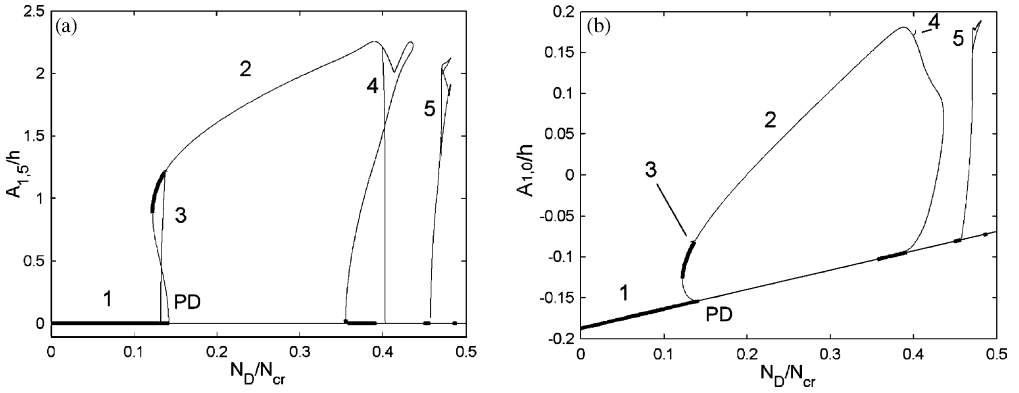

Fig. 4. Dynamic bifurcation (empty shell): static load $N/N_{cr} = 0.8$. (—) stable solution, (—) unstable solution.

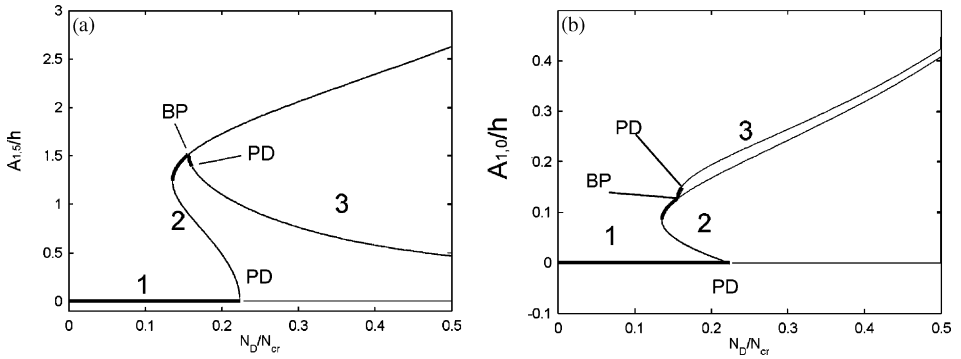

Fig. 5. Dynamic bifurcation (empty shell): membrane theory for in-plane stresses, static load $N/N_{cr} = 0.8$. (—) stable solution, (—) unstable solution; 'BP' bifurcation point, 'PD' period doubling.

companion mode, appears. Branch 3 loses stability at $N_D/N_{cr} = 0.161$ through a further period doubling bifurcation, which has not been followed. The difference with Gonçalves and Del Prado (2000) is now increased, and is probably due to the boundary conditions and the larger mode expansion used in the present study.

This analysis show that the postcritical scenario strongly depends on the approximations made in solving the governing equations: membrane theory, truncation of the series expansion and approximation of boundary conditions; furthermore, probably the shell theory used in the analysis could play an important role. Therefore, in the clarification of the complete postbifurcation scenario, both further theoretical refinements and laboratory experiments should be useful.

The damping model used in Popov et al. (1998) and Gonçalves and Del Prado (2000) seems to be not realistic. Indeed, experiments show that: (i) the damping ratio presents a different distribution over the modes with respect to the Kelvin–Voight model; (ii) the damping coefficient is usually smaller than 0.089, i.e., is of order of 10^{-4}, for empty shells, and 10^{-3}, for water-filled, stainless steel suspended shells having small dissipation at the edges (Amabili et al., 2002).

Some calculations are now made by assuming smaller value of the damping ratio; specifically, $\zeta = 0.0008$ for empty shell and $\zeta = 0.003$ for water-filled shell.

In Fig. 6(a)–(c) the maximum amplitude of oscillation of modes $A_{1,5}$, $B_{1,5}$ and $A_{1,0}$ versus N_D/N_{cr} is presented for an empty shell subjected to a periodic axial load having zero mean value ($N = 0$), $\zeta = 0.0008$

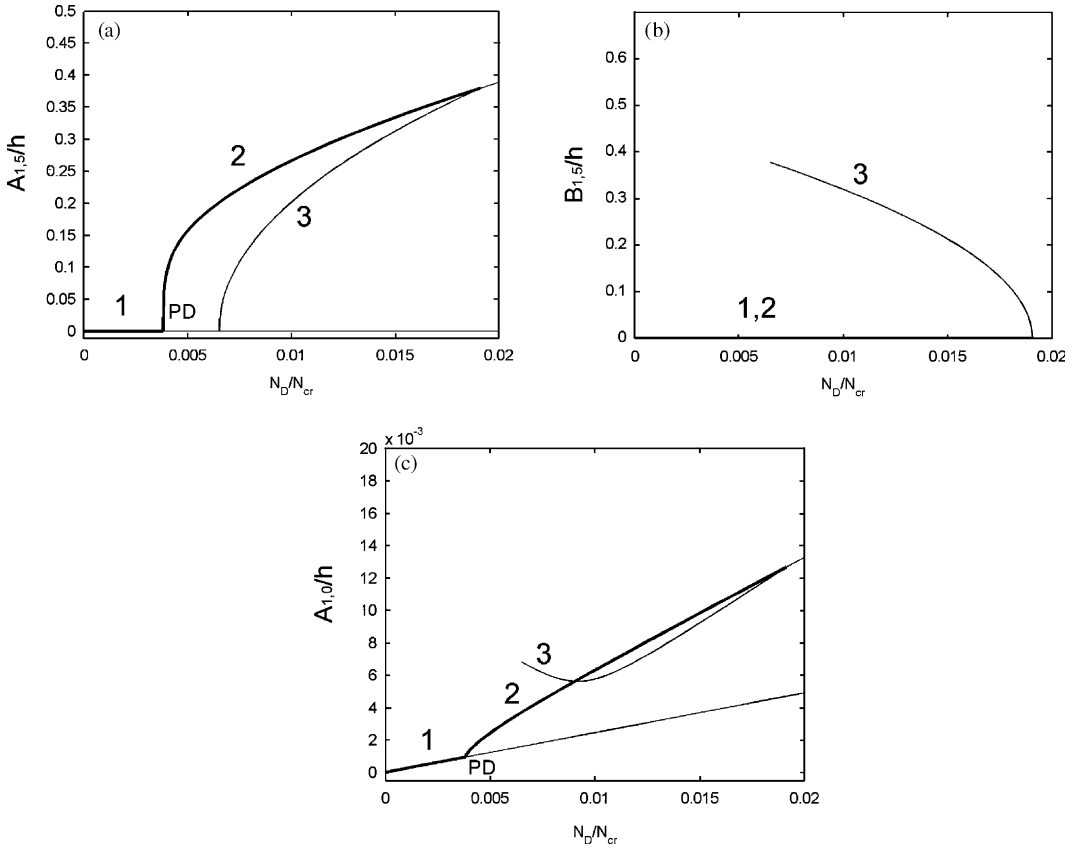

Fig. 6. Dynamic bifurcation: static load $N/N_{cr} = 0$, $\zeta = 0.0008$ (empty shell); (▬) stable solution, (—) unstable solution; 'PD' period doubling.

on all modes and $\omega/\omega_{1,5} = 2$. The scenario is changed with respect to the more damped cases, previously studied in Fig. 2. No sub-critical behaviour is present; however, the instability is reached for a smaller value of the excitation amplitude: $N_D/N_{cr} = 0.003$; for this excitation level a period doubling bifurcation takes place and originates the response represented by branch 2. The period $2T$ solution is stable up to $N_D/N_{cr} = 0.0191$, where the companion mode is excited through a bifurcation (branch 3); after this load no stable solutions are found.

The response of the empty shell is now analysed by varying the excitation frequency; the following parameters are considered: static load $N/N_{cr} = 0$; $N_D/N_{cr} = 0.01$; $\zeta = 0.0008$. In Fig. 7 a strong softening behaviour is observed (sub-critical bifurcation); when $\omega/\omega_{1,5} \cong 2$ the periodic response, which affects the axisymmetric modes only, undergoes to a period doubling bifurcation and gives rise to a period doubling solution. In the narrow region $\omega/\omega_{1,5} \in (1.774, 1.776)$ the sub-harmonic response presents a further bifurcation, which gives rise to the excitation of the companion mode $B_{1,5}$, see Fig. 7(b) and the picture included in Fig. 7(a); the axisymmetric mode generally follows the behaviour of asymmetric modes, Fig. 7(c).

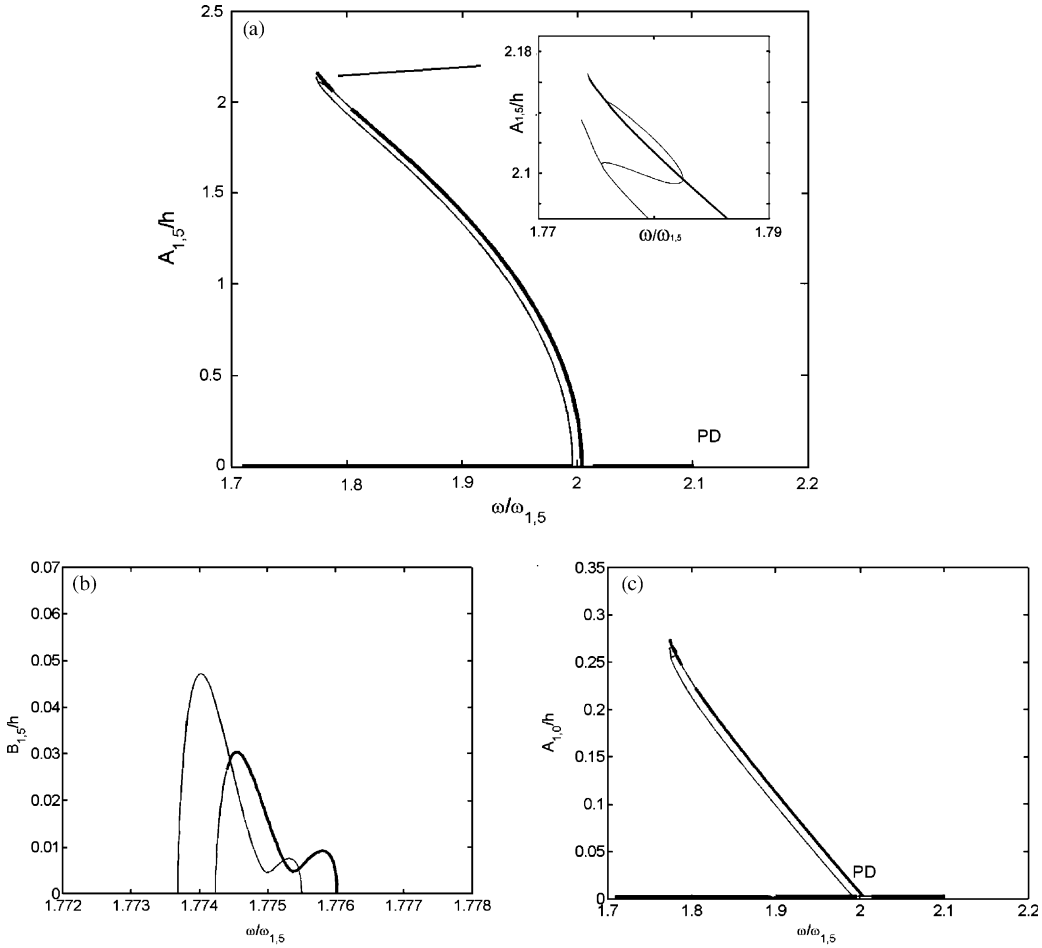

Fig. 7. Dynamic bifurcation (empty shell): dynamic load $N_D/N_{cr} = 0.01$, static load $N/N_{cr} = 0$, $\zeta = 0.0008$. (▬) stable solution, (—) unstable solution; 'PD' period doubling.

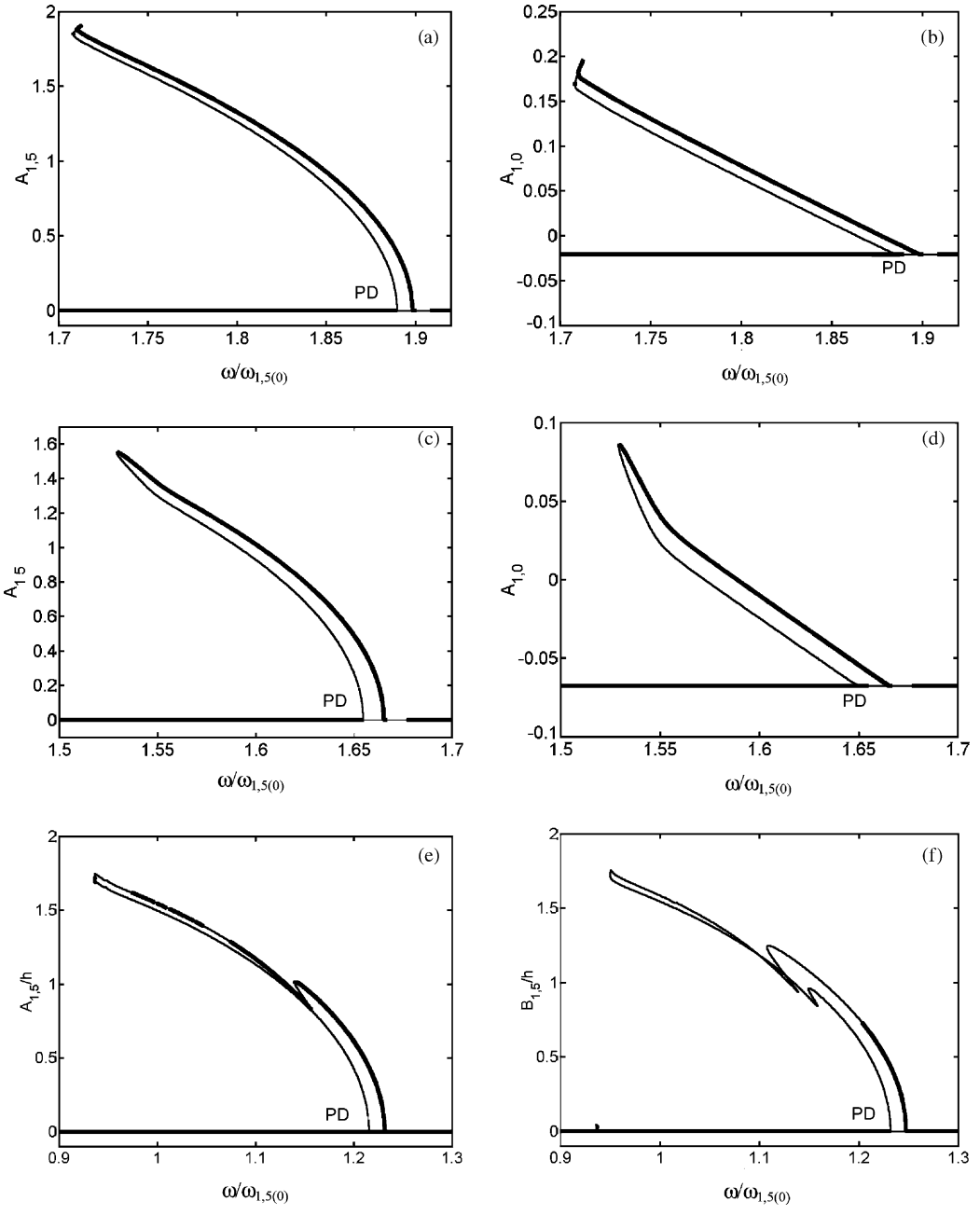

Fig. 8. Dynamic bifurcation (empty shell): (a,b) $N/N_{cr} = 0.1$, $N_D/N_{cr} = 0.01$; (c,d) $N/N_{cr} = 0.3$, $N_D/N_{cr} = 0.01$; (e,f) $N/N_{cr} = 0.6$, $N_D/N_{cr} = 0.01$. Damping ratio $\zeta = 0.0008$; (▬) stable solution, (—) unstable solution; 'PD' period doubling.

Increasing the static load N the scenario is changed; the case $N/N_{cr} = 0.1$, $N_D/N_{cr} = 0.01$, is represented in Fig. 8(a) and (b), and $N/N_{cr} = 0.3$, $N_D/N_{cr} = 0.01$ in Fig. 8(c) and (d); the damping ratio is $\zeta = 0.0008$. The case $N_D/N_{cr} = 0.01$, static load $N/N_{cr} = 0.6$, $\zeta = 0.0008$ is shown in Fig. 8(e) and (f). In the latter case, the trivial solution loses stability in the intervals: $\omega/\omega_{1,5(0)} \in (1.215, 1.231)$ and (1.232, 1.247). Mode $A_{1,5}$

bifurcates at $\omega/\omega_{1,5(0)} = 1.215$ (unstable branch) and $\omega/\omega_{1,5(0)} = 1.231$ (stable branch); conversely mode $B_{1,5}$ bifurcates at $\omega/\omega_{1,5(0)} = 1.232$ (unstable branch) and $\omega/\omega_{1,5(0)} = 1.247$ (stable branch). Modes $A_{1,5}$ and $B_{1,5}$ are never excited together, therefore, no travelling-wave motion appears. The bifurcation branch of $A_{1,5}$ is interesting; the following phenomena are present: folding at $\omega/\omega_{1,5(0)} = 1.14$ and 1.157; a region of alternate stable and unstable solutions bounded by torus bifurcations $\omega/\omega_{1,5(0)} \in (0.974, 1.074)$. Bifurcation solutions are present up to the frequency ratio $\omega/\omega_{1,5(0)} = 0.94$.

It is of interest to investigate the locus of the principal parametric instability by performing a two parameter continuation; the following parameters are considered in the continuation: $\omega/\omega_{1,5}$ and N_D/N_{cr}. The static load N/N_{cr} is assumed equal to zero and the damping ratio is $\zeta = 0.0008$, empty shell. In Fig. 9 the locus of period doubling looks quite interesting; the classical picture is found close to $\omega/\omega_{1,5} = 2$. However, many spikes are found for high values of N_D/N_{cr} and $\omega/\omega_{1,5} > 2$, which are probably due to the modal interactions.

The results reported in Fig. 6 show that no stable solutions are found for $N_D/N_{cr} > 0.0191$. In order to investigate the behaviour of the empty shell in this region a direct simulation is performed assuming: static load $N/N_{cr} = 0$, dynamic load $N_D/N_{cr} = 0.02$, damping ratio $\zeta = 0.0008$, excitation frequency $\omega/\omega_{1,5} = 2$; a 1% perturbation on the companion mode frequency is introduced in order to reproduce the same conditions of previous AUTO computations. An initial condition different from zero on $A_{1,5}$ is given. In Fig. 10 it can be seen that, after a very long time integration, $A_{1,5}$ reaches zero and the companion mode $B_{1,5}$ presents

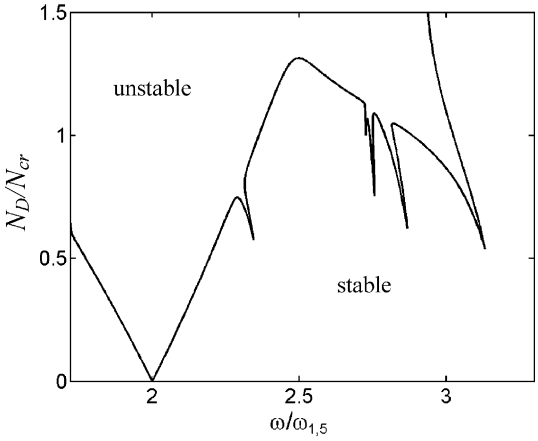

Fig. 9. Locus of period doubling: static load $N/N_{cr} = 0$, $\zeta = 0.0008$ (empty shell).

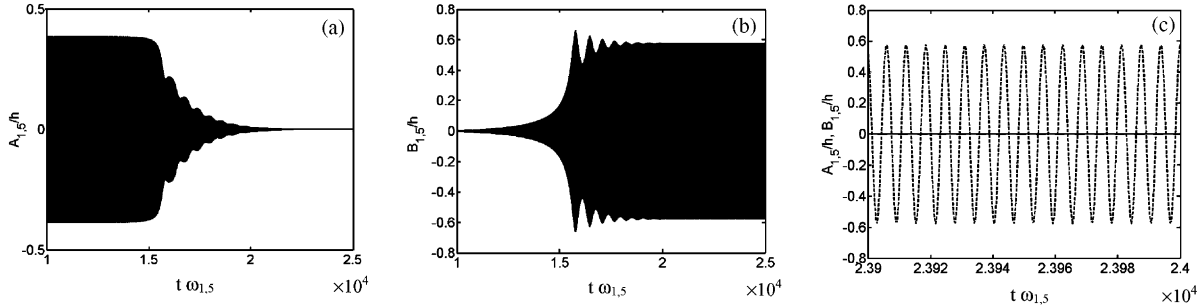

Fig. 10. Direct simulation (empty shell): static load $N/N_{cr} = 0$, $N_D/N_{cr} = 0.02$; $\zeta = 0.0008$, $\omega/\omega_{1,5} = 2$. (a) $A_{1,5}$, (b) $B_{1,5}$, (c) (—) $A_{1,5}$ and (— —) $B_{1,5}$. Perturbation on the companion mode frequency 1%.

a large amplitude of oscillation. This simulation shows that, for $N_D/N_{cr} > 0.0191$, stable periodic oscillations exist, but the role of $A_{1,5}$ and $B_{1,5}$ is exchanged.

In Fig. 11 the response of a water-filled shell is shown: the critical dynamic load is met at $N_D/N_{cr} = 0.296$ when $\zeta = 0.003$ on all modes and $\omega/\omega_{1,5} = 2$; the bifurcation is initially slightly sub-critical and unstable, indeed, a saddle node bifurcation (folding in Fig. 11(a)) is present at $N_D/N_{cr} = 0.28$. After this point the response becomes stable, and looses again stability at $N_D/N_{cr} = 0.67$, where the conjugate mode can be activated through a bifurcation (this branch has not been followed).

Periodic and nonstationary responses are now analyzed in detail by means of direct simulations and bifurcation diagram of Poincaré maps. The case of an empty shell is shown in Fig. 12; the following parameters are considered: $N/N_{cr} = 0.6$, $N_D/N_{cr} = 0.01$; $\zeta = 0.0008$. The diagram is obtained by decreasing the excitation frequency. A 1% perturbation of the natural frequency of the companion mode is used. At $\omega/\omega_{1,5(0)} = 1.251$ the parametric instability of the companion mode $B_{1,5}$ is met; indeed, because of the small perturbation, the natural frequency of the companion mode is 1% higher than the natural frequency of mode $A_{1,5}$. At $\omega/\omega_{1,5(0)} = 1.207$ the mode $A_{1,5}$ is excited and, for $\omega/\omega_{1,5(0)} = 1.157$, mode $B_{1,5}$ collapses to the trivial solution. In the region $\omega/\omega_{1,5(0)} \in (0.996, 1.077)$ alternate periodic and quasi-periodic orbits can be found. At $\omega/\omega_{1,5(0)} = 0.975$ a sudden jump to a chaotic orbit is found. At $\omega/\omega_{1,5(0)} = 0.929$ a jump to an orbit around the bifurcated static position takes place; the amplitude of oscillation is quite large (not shown), i.e. the shell collapses.

The periodic oscillations of the water-filled shell are now analysed. The following parameters are considered: $N/N_{cr} = 0.6$, $N_D/N_{cr} = 0.02$; $\zeta = 0.003$; where the bifurcation parameter is $\omega/\omega_{1,5(0)}$. A 1% perturbation is introduced, as previously done; the software AUTO is used. In Fig. 13(a) and (b) the amplitude of oscillation versus the excitation frequency, normalized with respect to the linear frequency $\omega_{1,5(0)}$ of the unloaded shell, is shown. Starting the simulation with a low frequency excitation $\omega/\omega_{1,5(0)} = 0.6$, the shell vibrates with the same frequency of the excitation ($1T$ oscillation). In particular, the asymmetric modes do not vibrate and the shell oscillation is completely axial–symmetric. The axisymmetric modes vibrate, but their amplitude is not shown for the sake of brevity. When $\omega/\omega_{1,5(0)} = 1.213$ the $1T$ oscillation loses stability and a period doubling bifurcation gives rise to branch 2, which represents the amplitude of a subharmonic ($2T$) response; the companion mode is not excited; this branch is completely unstable. Increasing the excitation frequency a second bifurcation is met at $\omega/\omega_{1,5(0)} = 1.23$, branch 4 (Fig. 13(b)); in this case the mode $B_{1,5}$ bifurcates; the frequency of mode $B_{1,5}$ is larger than mode $A_{1,5}$ because of the linear perturbation. Branch 4 shows a completely unstable bifurcation path. When $\omega/\omega_{1,5(0)} = 1.234$ a third

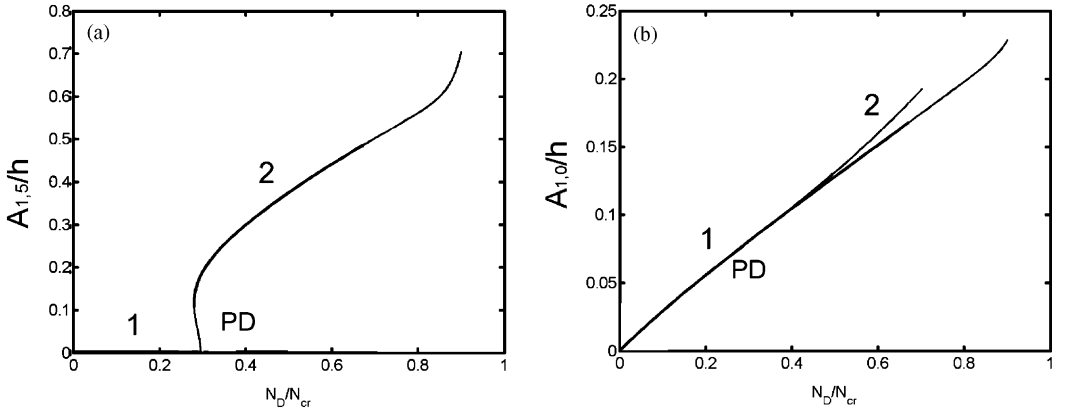

Fig. 11. Dynamic bifurcation: static load $N/N_{cr} = 0$, $\zeta = 0.003$ (water-filled shell); (━) stable solution, (—) unstable solution; 'PD' period doubling.

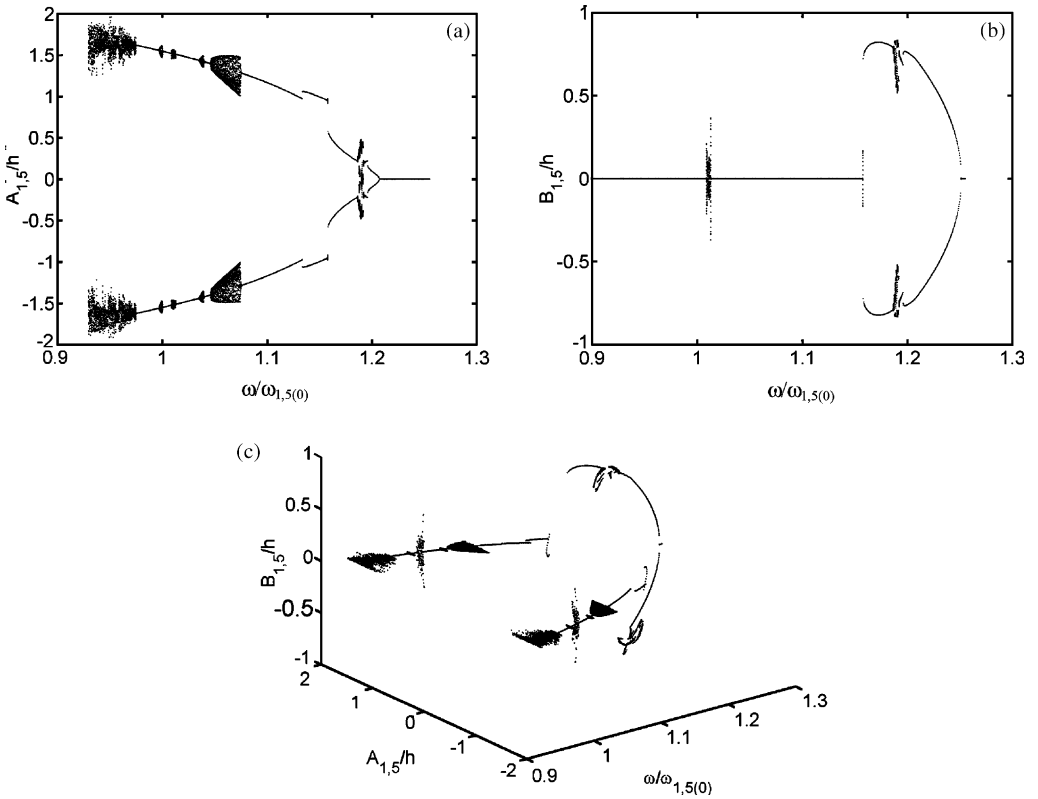

Fig. 12. Bifurcation diagram (empty shell): dynamic load $N_D/N_{cr} = 0.01$, static load $N/N_{cr} = 0.6$, $\zeta = 0.0008$. 1% perturbation on the linear frequencies.

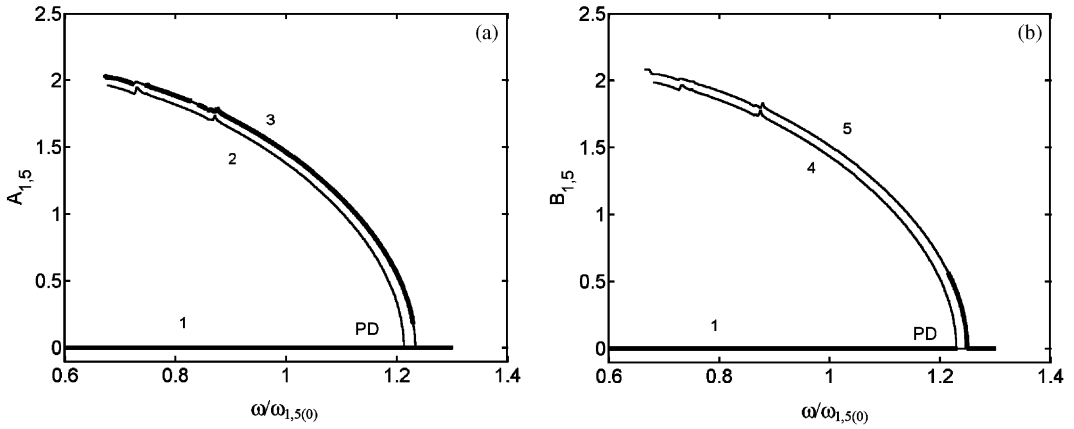

Fig. 13. Dynamic bifurcation (water-filled shell): dynamic load $N_D/N_{cr} = 0.02$, static load $N/N_{cr} = 0.6$, $\zeta = 0.003$. (━) stable solution, (—) unstable solution; 'PD' period doubling.

bifurcation takes place, involving mode $A_{1,5}$ (branch 3). The response is initially unstable and regains stability at $\omega/\omega_{1,5(0)} = 1.23$. Moreover, branch 3 presents a sequence of stable and unstable regions for

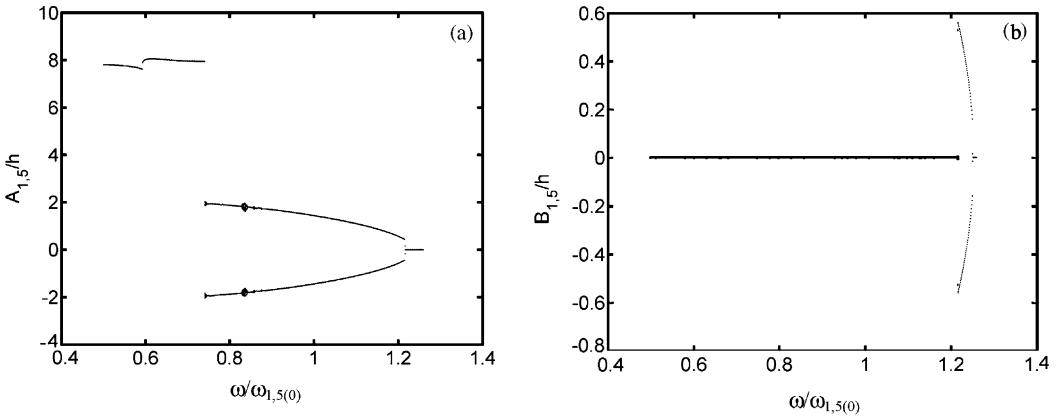

Fig. 14. Bifurcation diagram static load $N/N_{cr} = 0.6$, $N_D/N_{cr} = 0.02$, $\zeta = 0.003$ (water-filled shell).

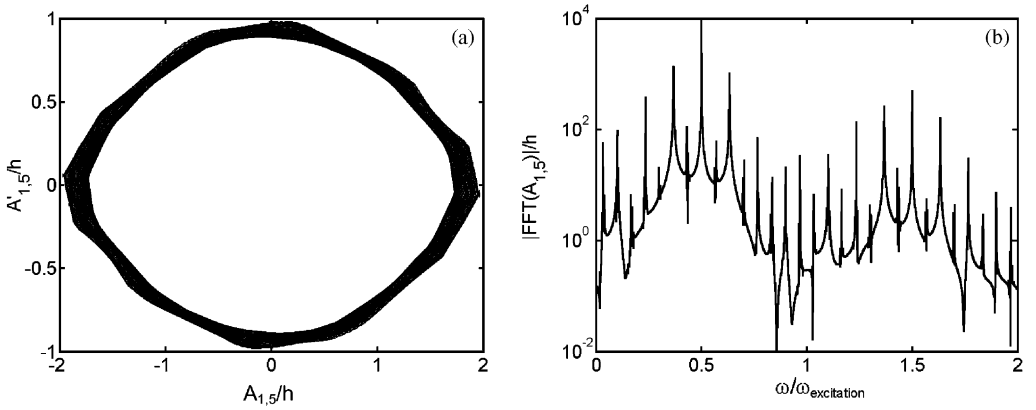

Fig. 15. Quasi-periodic motion: static load $N/N_{cr} = 0.6$, $N_D/N_{cr} = 0.02$; $\omega/\omega_{1,5(0)} = 0.8355$, $\zeta = 0.003$ (water-filled shell). (a) Projection of the phase space on the plane $(A_{1,5}, \dot{A}_{1,5})$, (b) spectrum of the time history of $A_{1,5}$.

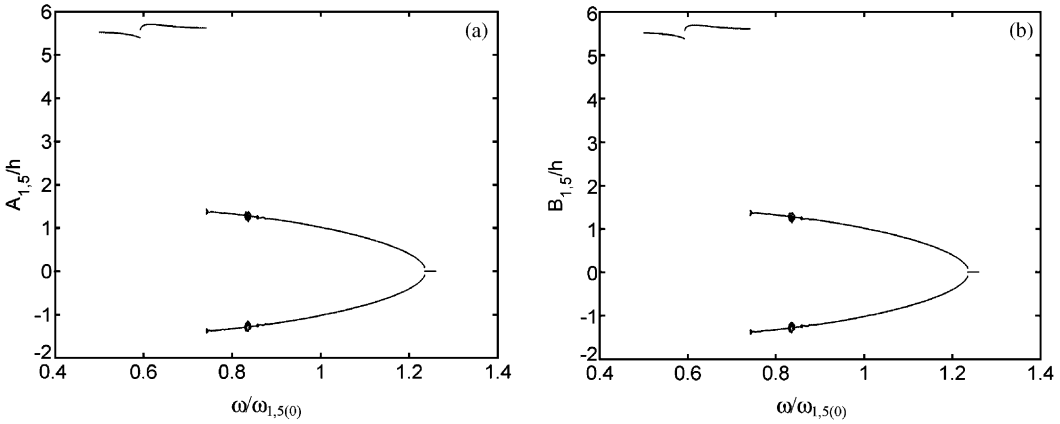

Fig. 16. Bifurcation diagram: static load $N/N_{cr} = 0.6$, $N_D/N_{cr} = 0.02$, $\zeta = 0.003$ (water-filled shell). No perturbation of the natural frequency of the companion mode. (a) Driven mode, (b) companion mode.

$\omega/\omega_{1,5(0)} \in (0.672, 0.876)$, bounded by torus bifurcation points. A fourth bifurcation is met at $\omega/\omega_{1,5(0)} = 1.249$, branch 5, involving mode $B_{1,5}$. Such solution is initially stable but loses stability at $\omega/\omega_{1,5(0)} = 1.215$, i.e., close to the first bifurcation of mode $A_{1,5}$. It is to note that the bifurcation paths are strongly sub-critical and the sub-harmonic response exist for a large range of the excitation frequency.

In order to investigate more deeply the numerical results obtained with the continuation technique, direct simulations are performed. In particular, the bifurcation diagram of Poincaré maps for the water-filled shell is shown in Fig. 14; the following parameters are considered: $N/N_{cr} = 0.6$, $N_D/N_{cr} = 0.02$; $\zeta = 0.003$. The diagram is obtained by decreasing the excitation frequency; indeed, the analysis of periodic solutions suggests the presence of a sub-critical bifurcation. A 1% perturbation is introduced, as in the previous computations, in order to reproduce the conditions of the simulations presented in Fig. 13. At $\omega/\omega_{1,5(0)} = 1.252$ the parametric instability of the companion mode is met; because of the small perturbation, the natural frequency of the companion mode $B_{1,5}$ is 1% higher than the natural frequency of mode $A_{1,5}$. At $\omega/\omega_{1,5(0)} = 1.217$ the orbit loses stability and the mode $A_{1,5}$ is excited. In the region $\omega/\omega_{1,5(0)} \in (0.83, 0.88)$ a quasi-periodic motion is found. A similar scenario is found close to

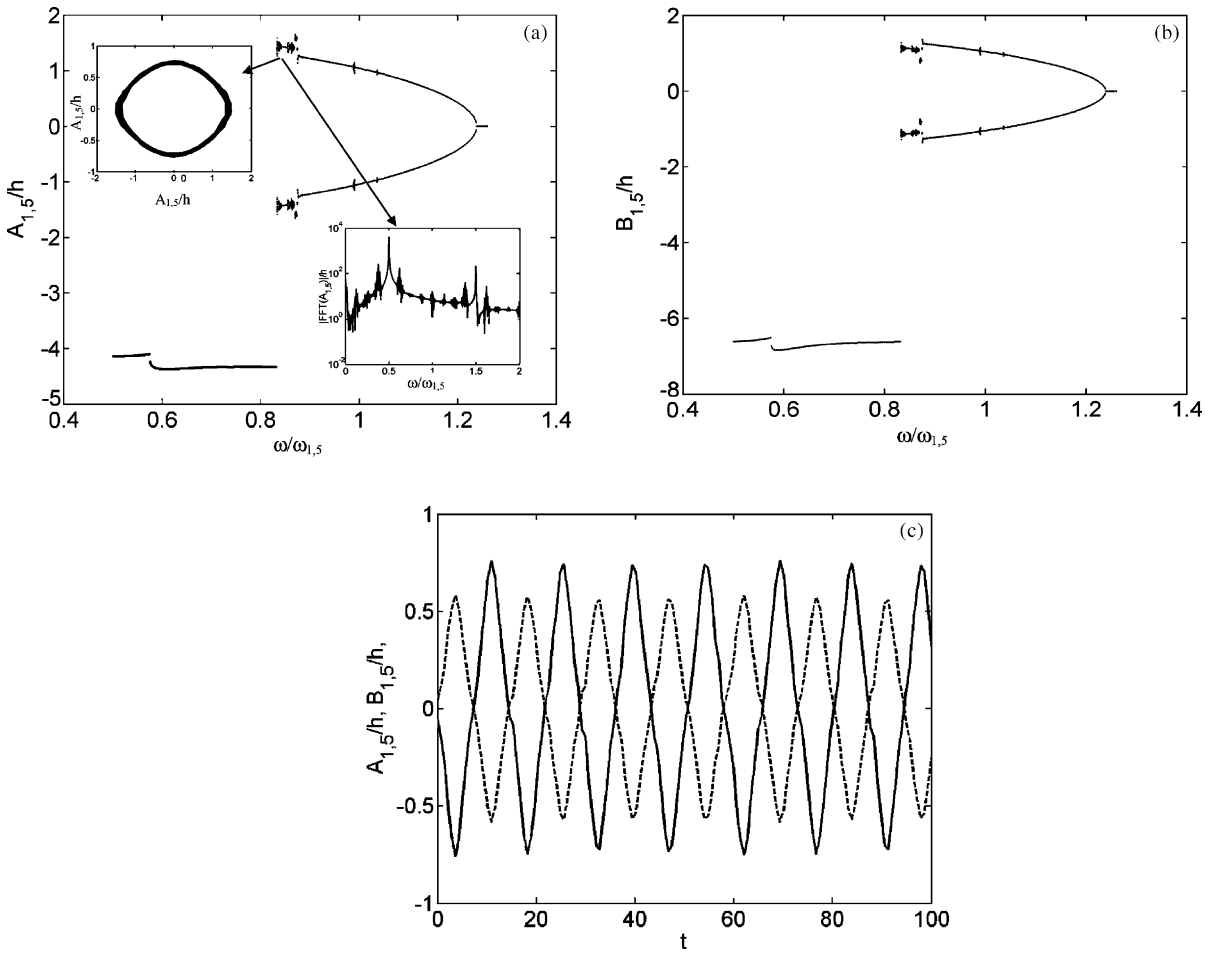

Fig. 17. Bifurcation diagrams and time histories: static load $N/N_{cr} = 0.6$, $N_D/N_{cr} = 0.02$, $\zeta = 0.001$ (water-filled shell), no perturbation of the natural frequency of the companion mode. (a) Bifurcation diagram of driven mode, (b) bifurcation diagram of companion mode, (c) time histories of driven and companion modes.

$\omega/\omega_{1,5(0)} = 0.74$; here a quasi-periodic orbit takes place, but it loses immediately stability and the system jump to a period-one orbit around the bifurcated static solution; the amplitude of oscillation is quite large, i.e. the structure is collapsed.

In order to investigate the shell motion in the narrow region where the quasi-periodic motion is found in the bifurcation diagram, direct simulations are performed for the water-filled shell using the following parameters: $N/N_{cr} = 0.6$, $N_D/N_{cr} = 0.02$; $\omega/\omega_{1,5(0)} = 0.8355$; $\zeta = 0.003$. In Fig. 15(a) the projection of the phase space on the plane $(A_{1,5}, \dot{A}_{1,5})$ shows that the trajectory is not closed and fill a part of the phase space. The spectrum, Fig. 15(b), shows a main 1/2 sub-harmonic component and a general splitting of harmonics, which is due to the modulation of amplitude. Note that in abscissa of Fig. 15(b), ω indicates the spectral line frequency and $\omega_{excitation}$ indicates the excitation frequency (the notation has been changed with respect to previous analyses).

Finally, in order to clarify the effect of linear perturbation introduced in the previously mentioned analyses, a perfect shell without linear perturbation is studied through direct simulations. Fig. 16(a) and (b) show that the behaviour is not very different from the perturbed case, shown in Fig. 14. However, now the linear frequency of modes $A_{1,5}$ and $B_{1,5}$ is the same, therefore both modes are symmetrically excited. The same problem is analysed in Fig. 17(a) and (b) for a smaller damping ratio: $\zeta = 0.001$; this simulation is performed to show the effect of a damping ratio reduction. It can be observed that the scenario is slightly changed; amplitude modulations appear in a larger range, but the overall behaviour is almost unchanged. In order to complete the analysis within Fig. 17(a) phase spaces and spectrum of $A_{1,5}$ are shown for $\omega/\omega_{1,5(0)} = 0.8606$ and in Fig. 17(c) the time histories of $A_{1,5}$ and $B_{1,5}$ are given. In particular it can be noted that the time histories of $A_{1,5}$ and $B_{1,5}$ have a phase difference $\theta \approx \pi$, which means that no pure travelling waves appear (see e.g. Amabili et al., 1999a, for the travelling-wave analysis).

6. Conclusions

The parametric instability and the postcritical behaviour of a circular cylindrical shell subjected to dynamic axial loads is analysed. The Donnell's nonlinear shallow-shell theory has been used, and partial differential equations have been discretized by means of the Galerkin procedure, using a relatively large set of modes in the expansion. The static buckling of a simply supported shell has been analysed and the results have been compared with the one present in the literature. Then, the combined effect of a static axial preload and dynamic loading is considered, in order to investigate the stability bounds and postcritical behaviour. Dynamic stability bounds for empty shells are compared with the results present in literature. The presence of a liquid gives rise to an increment of the linear damping and an added mass effect, which reduces the linear natural frequencies of vibration. The contained liquid causes interesting variations in the dynamic stability bounds. If the shell ends are open, the static stability and the static postcritical path are not influenced from the fluid-mass effect; indeed, it can be shown that the fluid contribution affects the inertial properties only. The role of axisymmetric dynamics has been investigated, showing the limitations of the membrane stress assumptions when the frequency of the periodic axial load approaches the frequency of axisymmetic modes. The role of the parametric resonance in the structural collapse has been confirmed both for empty and liquid filled shells.

Acknowledgements

This work was partially supported by the CNR Agenzia 2000 grant and NATO Cooperative Linkage Grant Project (N. PST.CLF. 977350).

References

Amabili, M., Païdoussis, M.P., 2003. Review of studies on geometrically nonlinear vibrations and dynamics of circular cylindrical shells and panels, with and without fluid–structure interaction. Applied Mechanics Reviews 56 (3).

Amabili, M., Pellicano, F., 2002. Multi-mode approach to nonlinear supersonic flutter of imperfect circular cylindrical shells. Journal of Applied Mechanics 69, 117–129.

Amabili, M., Pellicano, F., Païdoussis, M.P., 1998. Nonlinear vibrations of simply supported, circular cylindrical shells, coupled to quiescent fluid. Journal of Fluids and Structures 12, 883–918.

Amabili, M., Pellicano, F., Païdoussis, M.P., 1999a. Non-linear dynamics and stability of circular cylindrical shells containing flowing fluid. Part I: Stability. Journal of Sound and Vibration 225, 655–699.

Amabili, M., Pellicano, F., Païdoussis, M.P., 1999b. Non-linear dynamics and stability of circular cylindrical shells containing flowing fluid, Part II: Large-amplitude vibrations without flow. Journal of Sound and Vibration 228, 1103–1124.

Amabili, M., Pellicano, F., Païdoussis, M.P., 2000a. Non-linear dynamics and stability of circular cylindrical shells containing flowing fluid. Part III: Truncation effect without flow and experiments. Journal of Sound and Vibration 237, 617–640.

Amabili, M., Pellicano, F., Païdoussis, M.P., 2000b. Non-linear dynamics and stability of circular cylindrical shells containing flowing fluid. Part IV: Large-amplitude vibrations with flow. Journal of Sound and Vibration 237, 641–666.

Amabili, M., Pellicano, F., Vakakis, A.F., 2000c. Nonlinear vibrations and multiple resonances of fluid-filled, circular shells, Part 1: Equations of motion and numerical results. ASME Journal of Vibration and Acoustics 122, 346–354.

Amabili, M., Pellegrini, M., Pellicano, F., 2002. Large-amplitude vibrations of empty and fluid-filled circular cylindrical shells with imperfections: theory and experiments. In: Proceedings of the Symposium on FSI, ASME Int. Mech. Eng. Congr. and Exp., 17–22 November, New Orleans, USA, vol. 3 on CD-ROM (paper IMECE2002-39033).

Argento, A., 1993. Dynamic stability of a composite circular cylindrical shells subjected to combined axial and torsional loading. Journal of Composite Materials 27, 1722–1738.

Argento, A., Scott, R.A., 1993a. Dynamic instability of layered anisotropic circular cylindrical shells, Part I: Theoretical developments. Journal of Sound and Vibration 162, 311–322.

Argento, A., Scott, R.A., 1993b. Dynamic instability of layered anisotropic circular cylindrical shells, Part II: Numerical results. Journal of Sound and Vibration 162, 323–332.

Bert, C.W., Birman, V., 1988. Parametric instability of thick, orthotropic, circular cylindrical shells. Acta Mechanica 71, 61–76.

Croll, J.G.A., Batista, R.C., 1981. Explicit lower bounds for the buckling of axially loaded cylinders. International Journal of Mechanical Science 23 (6), 331–343.

Doedel, E.J., Champneys, A.R., Fairgrieve, T.F., Kuznetsov, Y.A., Sandstede, B., Wang, X., 1998. AUTO 97: Continuation and Bifurcation Software for Ordinary Differential Equations (with HomCont). Concordia University, Montreal, Canada.

Dowell, E.H., Ventres, C.S., 1968. Modal equations for the nonlinear flexural vibrations of a cylindrical shell. International Journal of Solids and Structures 4, 975–991.

Evensen, D.A., 1967. Nonlinear flexural vibrations of thin-walled circular cylinders. NASA TN D-4090, Government Printing Office, Washington, DC.

Gonçalves, P.B., Batista, R.C., 1988. Non-linear vibration analysis of fluid-filled cylindrical shells. Journal of Sound and Vibration 127, 133–143.

Gonçalves, P.B., Del Prado, Z.J.G.N., 2000. The role of modal coupling on the non-linear response of cylindrical shells subjected to dynamic axial loads. In: Proc. of the Symp. on Nonlinear Dynamics of Shells and Plates, ASME Int. Mech. Eng. Congr. and Exp., Orlando, USA, AMD Vol. 238. pp. 105–116.

Gonçalves, P.B., Del Prado, Z.J.G.N., 2002. Nonlinear oscillations and stability of parametrically excited cylindrical shells. Meccanica 37, 569–597.

Greenberg, J.B., Stavsky, Y., 1980. Buckling and vibration of orthotropic composite cylindrical shells. Acta Mechanica 36, 15–29.

Hsu, C.S., 1974. On parametric excitation and snap-through stability problems of shells. In: Fung, Y.C., Sechler, E.E. (Eds.), Thin-Shell Structures. Theory Experiments and Design. Prentice-Hall, Englewood Cliffs, NJ.

Koval, L.R., 1974. Effect of longitudinal resonance on the parametric stability of an axially excited cylindrical shell. Journal of Acoustic Society of America 55 (1), 91–97.

Koval'chuk, P.S., Krasnopol'skaya, T.S., 1980. Resonance phenomena in nonlinear vibrations of cylindrical shells with initial imperfections. Soviet Applied Mechanics 15, 867–872.

Kubenko, V.D., Koval'chuk, P.S., Krasnopol'skaya, T.S., 1982. Effect of initial camber on natural nonlinear vibrations of cylindrical shells. Soviet Applied Mechanics 18, 34–39.

Lakis, A.A., Laveau, A., 1991. Non-linear dynamic analysis of anisotropic cylindrical shells containing a flowing fluid. International Journal of Solids and Structures 28, 1079–1094.

Nagai, K., Yamaki, N., 1978. Dynamic stability of circular cylindrical shells under periodic compressive forces. Journal of Sound and Vibration 58 (3), 425–441.

Nayfeh, A.H., Mook, D.T., 1979. Nonlinear Oscillations. John Wiley & Sons, New York.

Pellicano, F., Amabili, M., Païdoussis, M.P., 2002. Effect of the geometry on the non-linear vibration of circular cylindrical shells. International Journal of Non-Linear Mechanics 80, 899–906.

Pellicano, F., Amabili, M., Vakakis, A.F., 2000. Nonlinear vibrations and multiple resonances of fluid-filled, circular shells, Part 2: Perturbation analysis. ASME Journal of Vibration and Acoustics 122, 355–364.

Popov, A.A., Thompson, J.M.T., McRobie, F.A., 1998. Low dimensional models of shell vibrations. Parametrically excited vibrations of cylindrical shells. Journal of Sound and Vibration 209, 163–186.

Roth, R.S., Klosner, J.M., 1964. Nonlinear response of cylindrical shells subjected to dynamic axial loads. AIAA Journal 2, 1788–1794.

Tamura, Y.S., Babcok, C.D., 1975. Dynamic stability of cylindrical shells under step loading. Journal of Applied Mechanics 42, 190–194.

Vijayaraghavan, A., Evan-Iwanowski, R.M., 1967. Parametric instability of circular cylindrical shells. Journal of Applied Mechanics 34, 985–990.

Von Kármán, T., Tsien, H.S., 1941. The buckling of thin cylindrical shells under axial compression. Journal of the Aeronautical Sciences 8 (8), 303–312.

Yamaki, N., 1984. Elastic Stability of Circular Cylindrical Shells. North-Holland, Amsterdam.